Importance of Fourth-Order Zero-Field Splitting Terms in Random-Orientation EPR Spectra of Eu(II)-Doped Strontium Aluminate

Hideto Matsuoka,[†] Ko Furukawa,[†] Kazunobu Sato,[‡] Daisuke Shiomi,[‡] Yoshitane Kojima,[‡] Ken Hirotsu,[‡] Nobuo Furuno,[§] Tatsuhisa Kato,*[,†] and Takeji Takui[‡]

Institute for Molecular Science, Okazaki National Research Institutes, Myodaiji, Okazaki 444-8585, Japan, Departments of Chemistry and Materials Science, Graduate School of Science, Osaka City University, Sugimoto 3-3-138, Sumiyoshi-Ku, Osaka 558-8585, Japan, and Fine Clay Co., Ltd., Osho-Kita 1−3−8, Amagasaki, Hyogo 660-0063, Japan

Received: June 30, 2003; In Final Form: October 15, 2003

This work discusses an issue caused by omitting the fourth-order zero-field splitting (ZFS) terms in the analysis of random-orientation EPR spectra. Eu(II)-doped strontium aluminates were employed as a model system of the S-state lanthanoid ions, which have relatively large second-rank ZFS components, comparable to the conventional X-band microwave energy. The initial estimation of second- and fourth-rank ZFS components was acquired uniquely from the W-band spectrum based on a perturbation treatment of the spin Hamiltonian, and they were refined by a hybrid-eigenfield simulation approach. A parallel simulation of the X- and W-band spectra with the refined parameters reasonably reproduced both the observed spectra. The reliability of the parameters was also verified by reproducing the off-principal-axis extra lines arising from the $M_S = 1/2 \leftrightarrow -1/2$ transition observed in the W-band spectrum. By comparison with an analysis based on the spin Hamiltonian omitting the fourth-order terms, it was concluded that omitting these terms results in an erroneous determination of the rhombic parameter (E) of the second-rank ZFS tensor. The obtained reliable second-rank ZFS tensors enabled us to invoke the superposition model, determining their principal-axis orientation. This is the first report of such relative orientation determined for Eu(II)-doped strontium aluminates.

Introduction

In material and biological sciences, random-orientation electron paramagnetic resonance (EPR) spectroscopy has been widely used to explore electronic and molecular structures of spin systems that are hard to obtain in a single-crystal form.[1,3] In random-orientation EPR spectroscopy, only dominant interactions in the spin Hamiltonian are generally considered in spectral analyses, for simplicity. Although the higher-order zero-field splitting (ZFS) terms are essential for high-spin systems with $S \geq 2$, they have been frequently neglected.[1,4−8] The terms arising from the higher-order spin−orbit perturbation are justifiably omitted for high-spin states of hydrocarbons because of small spin−orbit couplings.[1] On the other hand, it has been shown that the terms are crucial parameters for analyzing single-crystal EPR spectra observed for high-spin lanthanoid ions with large spin−orbit couplings. Nevertheless, some workers have assumed that the terms can be neglected even for such ions in random-orientation EPR spectroscopy.[4−8] This article demonstrates that the terms are crucial parameters even in random-orientation EPR spectroscopy.

Powder samples of Eu(II)-doped strontium aluminates were used as a model system. Their luminescent properties are also of great interest, and will be published elsewhere.[10] The ZFS parameters were evaluated directly from the experimental W-band EPR spectrum with the help of a perturbation treatment of the spin Hamiltonian considering all fourth-order terms. The parameters were refined by invoking computer simulation of the X- and W-band EPR spectra based on a hybrid-eigenfield approach, which we have proposed as a practical method for EPR spectral simulation.[1,9,11,12] To elucidate the importance of the fourth-order terms, the parametrization was also carried out by using the spin Hamiltonian without them. Comparing the two results, it is demonstrated that omission of the fourth-order terms results in a misestimation of the second-rank ZFS components, D and E. The importance of parametrization considering the fourth-order terms is also discussed in relation to an off-axis extra line from the $M_S = 1/2 \leftrightarrow -1/2$ transition observed in the W-band spectrum. This is the first report of the simulation completely considering the fourth-order terms as well as the central line structure due to the extra line.

Once a reliable second-rank ZFS tensor is obtained by a simulation considering the fourth-order terms, the orientation of the principal-axis can be determined. Theoretical interpretation of the ZFS for S-state ions has been a long-standing issue.[13] A variety of mechanisms contributing to the ZFS have been proposed so far: the spin−spin interaction,[14] the overlapping and covalent effects,[13,15] the relativistic effect,[16] and the spin−orbit interaction.[17] The exact treatment is complicated due to the competition and mutual cancellation of these mechanisms. On the other hand, the superposition model (SPM) is a straightforward manner to explain ZFS of S-state ions.[18] In this article, the principal-axis orientation is determined in the frame of the SPM.

Perturbation theory to estimate second- and fourth-rank ZFS components of $S = 7/2$ spins was described by Abraham et al.[19] They considered only b_4^0 and b_4^4 as the fourth-rank

* Corresponding author. Phone: +81-564-55-7330. Fax: +81-564-55-4639. E-mail: kato@ims.ac.jp.
[†] Institute for Molecular Science.
[‡] Osaka City University.
[§] Fine Clay Co., Ltd.

10.1021/jp030819+ CCC: $25.00
Published on Web 11/25/2003

components. They confirmed the validity of the analysis by comparing with single-crystal EPR studies. Koopmans et al. also demonstrated a parametrization procedure by the combined use of Abraham's approach and computer simulation based on numerical diagonalization of the spin Hamiltonian.[20] On the other hand, we reported another approach using the hybrid-eigenfield method instead of the numerical diagonalization.[21] In this work, the approach was extended by considering all fourth-order terms, and it can be addressed for other $S = 7/2$ systems.

Materials and Methods

Preparation and EPR Measurements. The particular size of sample particle was obtained by sieving.[10] The size distribution of the particle varies from 0.3 to 70 μm, in which about 70% of the components are smaller than 10 μm. The mean particle diameter is 6.8 μm. The particle shows the broad emission band centered at 490 nm.[10] The X-band CW EPR measurement was carried out at low temperature using a Bruker ESP300 spectrometer equipped by an Oxford 910 helium gas-flow temperature controller. Q- and W-band EPR measurements were carried out by Bruker E500 and E680 spectrometers, respectively. Temperature was controlled by an Oxford CF935 helium gas-flow cryostat.

Spectral Simulation. An EPR spectral simulation program based on a hybrid-eigenfield approach was constructed using MATLAB 6.5 provided by The MathWorks Inc. In this program, one can consider zero-field splitting (ZFS) terms up to sixth order, electronic Zeeman terms, nuclear Zeeman terms, hyperfine interaction terms, and nuclear quadrupole terms. In this work, the simulation program was run on a conventional personal computer with dual Intel Xeon 2.4 GHz processors. In the following, the principle of our spectral simulation algorithm is briefly described.

This program is composed of two major parts. The first part is to execute direct numerical computations of resonance fields without any iteration procedure, based on the eigenfield method originally developed by Belford et al.[22] The second part is to calculate the corresponding transition probabilities by numerically diagonalizing the eigen-energy matrix with the obtained resonance fields. We have proposed and developed this eigenfield and eigen-energy method,[1,9,11,12] and termed the "hybrid eigenfield approach".[1,9] The transition probability can be also calculated directly by the original eigenfield method. However, since the direct calculation requires solving a generalized eigenvalue problem of a complex matrix much larger than the eigen-energy matrix, an enormous computing time is consumed for acquiring the eigenvector with proper accuracy. For a large spin quantum number such as $S = 7/2$, the direct calculation is impractical for random-orientation fine-structure EPR spectroscopy. In addition, the accuracy depends on an algorithm employed for solving the complex eigenvalue problem. The hybrid approach enables us to calculate both resonance fields and transition probabilities in terms of both reasonable computational time and proper accuracy with eigenvectors. It also facilitates the consideration of the Boltzmann distribution in the simulation. Cugunov et al. also independently described the same idea, focusing only on the computing time (termed "combined method" in their paper).[23]

The theoretical powder-pattern EPR spectrum $S(B)$ is obtained by integrating all of the spectra from random orientations with respect to the static magnetic field, i.e.,

$$S(B) = \int_\theta \int_\phi (s, \theta, \sigma, B) \sin\theta \, d\theta\phi \qquad (1)$$

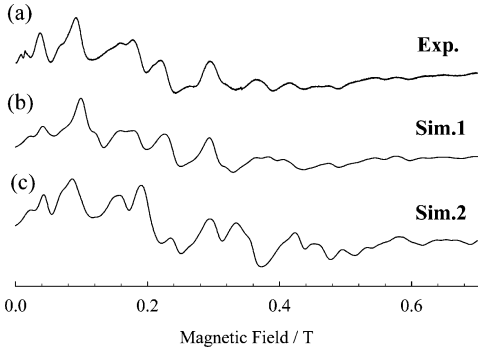

Figure 1. (a) X-band EPR spectra observed for the Eu(II) ions doped in strontium aluminates at $\nu = 9.60479$ GHz and 4 K. (b) Sim.1: X-band spectra calculated with the spin-Hamiltonian parameters in Table 1. (c) Sim.2: X-band spectra calculated with the spin-Hamiltonian parameters in Table 2.

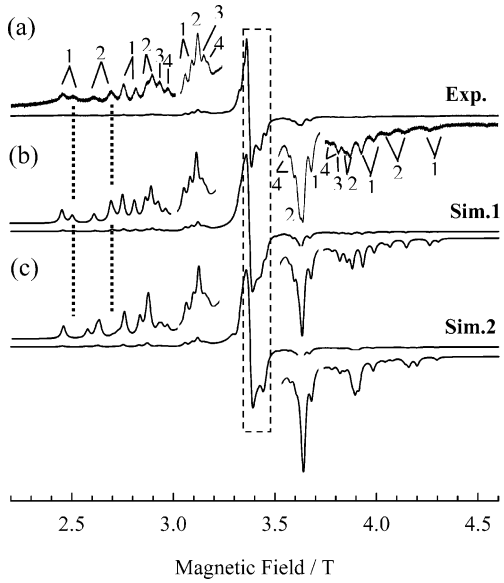

Figure 2. (a) W-band EPR spectra observed for the Eu(II) ions doped in strontium aluminates at $\nu = 94.08930$ GHz and 40 K. The transitions arising from the Eu(1), Eu(2), Eu(3), and Eu(4) sites are denoted by 1, 2, 3, and 4, respectively. (b) Sim.1: W-band spectra calculated with the spin-Hamiltonian parameters in Table 1. (c) Sim.2: W-band spectra calculated with the spin-Hamiltonian parameters in Table 2.

where θ, ϕ, andψ stand for the Euler angles. We have to perform the integration over only one octant for orthorhombic, two octants for monoclinic, and four octants for triclinic symmetries. To save computing time, the Igloo method developed by Belford et al. was utilized as an angular grid method.[3,24] Here, the spectrum pattern $s(\theta, \phi, B)$ is given by

$$s(\theta,\phi,B) = \sum_i f(B - B_i^{res}(\theta,\phi),\Delta B_{1/2}) \times \int P_i(\theta,\phi,\psi) \, d\psi \qquad (2)$$

where B_i^{res} stands for resonance fields, $\Delta B_{1/2}$ for the line width at half-height, P_i (θ, ϕ, ψ) for the transition probability, and f for an appropriate line shape. The Gaussian function, Lorentzian function, and a convolution of them (Voigt function) can be employed as the line shape.

Results

X and W-Band EPR Spectra Observed for Eu(II) Ions Doped in Strontium Aluminates. Figures 1a and 2a show the experimental X and W-band EPR spectra, respectively. The X-band spectrum exhibited an asymmetric spectral pattern due

to the relatively larger zero-field splitting (ZFS) term that is comparable to the X-band microwave energy. On the other hand, the W-band spectrum exhibited a symmetrical pattern that we can assign with ease, where the Zeeman term is considerably larger than the ZFS term. In the following, the parametrization procedures to extract the ZFS parameters directly from the W-band spectrum are described.

Estimation of the ZFS Parameters Based on Perturbation Treatment of the Spin Hamiltonian. Fine-structure EPR spectrum observed for a spin system with $S \geq 2$ can be interpreted by the following spin Hamiltonian:

$$\hat{H} = \beta_e \mathbf{S}\cdot\mathbf{g}\cdot\mathbf{B} + \sum_{k,q} f_k b_k^q O_k^q \quad (k = 2,4,6 \text{ and } k \geq |q|) \quad (3)$$

where the first term stands for the electron Zeeman interaction, and the remaining terms for the ZFS. The b_k^q values represent the ZFS parameter, and O_k^q is the Stevens operator (see Appendix). Since the operators at higher degree than 2*S* have zero matrix elements, the terms up to fourth-order require $S = 2$ and 5/2 system and those up to sixth-order require $S = 7/2$. The scaling factors f_k are chosen to be independent of q as follows:

$$f_2 = 1/3, \; f_4 = 1/60, \; f_6 = 1/1260$$

Since the scaling factors of the sixth-order terms are sufficiently small, they are neglected here.

Observable peaks in a random-orientation EPR spectrum are generally called canonical peaks, which are assigned to transitions observed with **B** oriented along the principal axis (*X*, *Y*, and *Z*) of the second-rank ZFS tensor. In the high-field approximation, seven allowed-transition peaks arise from the Eu(II) ion with $S = 7/2$ for each canonical line. Then twenty-one allowed transition peaks can be expected in the random-orientation EPR spectrum. The stick diagram in Figure 3a shows the field positions of the canonical peaks obtained for given values of g, b_2^0, b_2^2, b_4^0, b_4^2, and b_4^4 at 95 GHz. Here, the solid lines correspond to the *Z* canonical peaks and the dashed lines to the *Y* canonical peaks. For simplicity, canonical *X* peaks are not shown here. Also, the seven allowed transitions, $M_S - 1 \leftrightarrow M_S$, are designated by $(M_S - 1, M_S)$ on top of Figure 3. Under the first-order approximation, the six field separations shown by the arrows in Figure 3a are given by eqs A7 and A8 in the Appendix. Using these equations, the six parameters can be determined uniquely by adjusting those sticks to the peaks of the experimental W-band spectrum.[19,21] The approximate ZFS parameters of the sample were determined in this manner and then were refined with the help of the hybrid eigenfield method. Assuming four non-equivalent Eu(II) crystal sites in the sample, all peaks observed in the W-band spectrum were reproduced by the stick diagram. The determined parameters are shown in Table 1. The signs of the b_2^0 values were determined by analyzing the temperature dependence of the W-band spectra.[10]

As can be seen in eq A7, only the b_4^0 value among the fourth-rank ZFS components influences the field positions of the *Z* canonical peaks. On the other hand, the field positions of *Y* canonical peaks depend on all of the fourth-rank ZFS components. Therefore, an erroneous rhombic parameter ($E = 1/3b_2^2$) would be given by omitting the fourth-order terms in spectral analysis. To examine the issue, the second-rank ZFS components were estimated independently by using the simplified spin Hamiltonian:

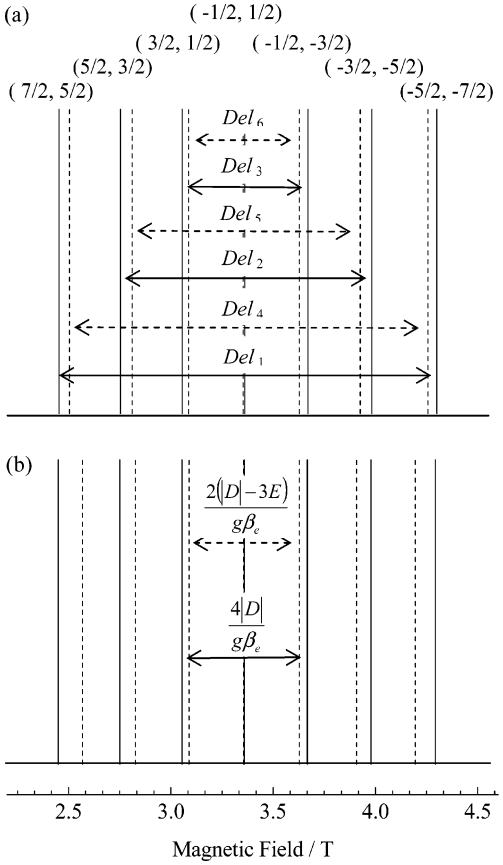

Figure 3. (a) Canonical peaks of allowed transitions arising from an $S = 7/2$ spin system obtained at 95 GHz using given values of g, b_2^0, b_2^2, b_4^0, b_4^2, and b_4^4. The seven allowed transitions, $M_S - 1 \leftrightarrow M_S$, are designated by $(M_S - 1, M_S)$. The transitions arising from the *Z* canonical orientation are shown by the solid lines, and those from the *Y* canonical orientation by dashed lines. (b) Canonical peaks of allowed transitions arising from an $S = 7/2$ spin system obtained at 95 GHz using given values of g, b_2^0, and b_2^2.

TABLE 1: Spin Hamiltonian Parameters Determined by the Analysis Incorporating the Fourth-Order Terms

	Eu(I)	Eu(2)	Eu(3)	Eu(4)
$g_\perp$	1.9938	1.9930	1.9921	1.9930
$g_\parallel$	1.9934	1.9912	1.9917	1.9952
b_2^0/cm^{-1}	−0.1435	0.1180	0.1043	0.1036
b_2^2/cm^{-1}	0.1225	0.1001	0.1011	0.0874
b_4^0/cm^{-1}	$<10^{-4}$	0.0002	0.0053	−0.001
b_4^2/cm^{-1}	0.0012	0.0084	−0.0022	0.0025
b_4^4/cm^{-1}	0.0093	−0.0019	−0.0012	−0.0064
intensity ratio	5	5	1	1

fied spin Hamiltonian:

$$\hat{H} = \beta_e \mathbf{S}\cdot\mathbf{g}\cdot\mathbf{B} + D\left[S_z^2 - \frac{1}{3}S(S+1)\right] + E[S_x^2 - S_y^2] \quad (4)$$

where the ZFS parameters D correspond to b_2^0 and E to $1/3b_2^2$, which are described in eq 3. The conventional spin Hamiltonian eq 4 has been used by some workers in analyses of powder-pattern EPR spectra arising from $S = 7/2$ spin systems.[4−8] Under the first-order approximation based on eq 4, the field separation between the two inner intense sidelines for the *Z* canonical peaks is given by $4|D|/g\beta_e$, as shown by solid lines in Figure 3b. Also, the separation between the two inner lines for the *Y* canonical peaks is given by $2(|D| - 3E)/g\beta_e$, as shown by dashed lines in Figure 3b. Consequently, approximate ZFS parameters were

TABLE 2: Spin Hamiltonian Parameters Determined by the Analysis Omitting the Fourth-Order Terms

	Eu(I)	Eu(2)	Eu(3)	Eu(4)
$g_\perp$	1.9930	1.9904	1.9887	1.9902
$g_\parallel$	1.9954	1.9894	1.9887	1.9932
b_2^0/cm^{-1}	−0.1433	0.1194	0.1070	0.1042
b_2^2/cm^{-1}	0.0197	0.01045	0.0979	0.0822
intensity ratio	5	5	1	1

determined from the two separations in the obtained spectrum. Assuming four non-equivalent Eu(II) sites, the approximate parameters were refined with the help of the hybrid-eigen field method. The determined parameters are shown in Table 2. Here, it should be noticed that the derived ZFS parameters were in disagreement with those in Table 1. In particular, there is the significant discrepancy between the b_2^2 values as predicted above. Also it is reasonable that the outermost peaks obtained by the methods based on the different approximation do not coincide with each other.

Discussion

Examination of the Reliability of the Determined ZFS Parameters Based on the Spectral Simulation. Figure 2b shows the W-band EPR spectrum calculated with the parameters in Table 1, which was obtained by superimposing the spectrum of four non-equivalent Eu sites with the intensity ratio of 5:5:1:1. The calculated spectrum reasonably reproduced the observed one. From the photoluminescence meaurement it was shown that the sample stoichometrically contained $SrAl_2O_4$:Eu,Dy and $Sr_4Al_{14}O_{25}$:Eu,Dy with the ratio of 5:1.[10] It was indicated by comparing with Nakamura's result[4c,4d] that the Eu(1) and Eu(2) sites are substituted for the two Sr sites in the $SrAl_2O_4$ host crystal and that the Eu(3) and Eu(4) sites are substituted for the two Sr sites in the $Sr_4Al_{14}O_{25}$ host crystal. These facts strongly support the assignment superimposing the spectrum of four non-equivalent Eu sites with the intensity ratio of 5:5:1:1.[26,27,33]

We also performed the spectral simulation of the corresponding X-band spectrum in order to examine the reliability of the parameters in Table 1. The result is shown in Figure 1b, which was in good agreement with the observed spectrum again. On the other hand, as shown in Figures 1c and 2c, the theoretical spectra based on the parameters in Table 2 were in disagreement with the corresponding experimental spectra. As mentioned above, the largest discrepancy is between the theoretical and experimental results for the outermost peaks. For example, the two peaks indicated by dotted lines in Figure 2a and 2b are missing in Figure 2c. As described in the Supporting Information, a similar discrepancy was found in the simulation analysis for the higher frequency (180 GHz) spectra reported by Nakamura et al.[4] As a result, it was shown that the experimental spectra are not completely reproduced by the spectral simulation unless the fourth-order terms are considered. Moreover, it was revealed that the omission of the terms results in the misevaluation of the E value.

Off-Principal-Axis Extra Peaks. To demonstrate the necessity of considering the fourth-order terms, we also examined off-principal-axis extra lines, which correspond to the transition observed with the magnetic field oriented along the directions of off-principal axes. It was shown by one of the authors that electronic high-spin systems with odd spin quantum numbers always give a characteristic peak of the extra line arising from the $M_S = 1/2 \leftrightarrow -1/2$ transition.[1,25] As shown in the Appendix, the fourth-rank ZFS components do not directly influence the field position the same manner as do the second-rank ZFS components.

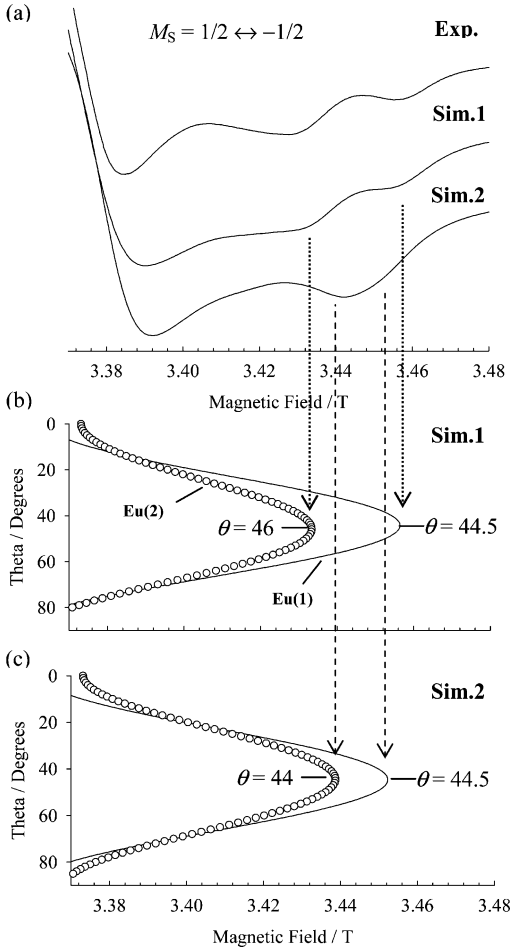

Figure 4. (a) Experimental and theoretical W-band spectra corresponding to the area surrounded by dashed lines in Figure 2. Only the $M_S = 1/2 \leftrightarrow -1/2$ transition appears in the field region. (b) Angular variation of the resonance fields calculated with the parameters in Table 1; $0 \le \theta \le \pi/2$ and $\phi = \pi/2$. (c) Angular variation of the resonance fields calculated with the parameters in Table 2; $0 \le \theta \le \pi/2$ and $\phi = \pi/2$. The solid lines represent the calculations for the Eu(1) site and the opened circles for the Eu(2) site.

Figure 4a corresponds to the area surrounded by dashed lines in Figure 2. Only the $M_S = 1/2 \leftrightarrow -1/2$ transition appears in the field region. The angular variation of the resonance field calculated with the parameters in Tables 1 and 2 are also shown in Figures 4b and 4c, respectively. The solid lines and opened circles represent the angular variations calculated for the Eu(1) and Eu(2) sites, respectively. As shown in the figure, the structure of the spectrum arises from the extra lines. It should be noticed that the structure due to the extra lines was observed even in higher frequency (180 GHz) EPR spectra, as shown in the Supporting Information. The misevaluation of D and E values reflected the position of the extra lines in a sensitive manner. As shown in Figure 4, the calculation with the parameters in Table 1 reasonably reproduced the observed extra lines, but the parameters in Table 2 did not give the proper position of the lines. Therefore, it is concluded that the second-rank ZFS components cannot be precisely determined by the spectral analysis without incorporating the fourth-rank ZFS components. The extra line analysis during the spectral simulation gives a useful testing ground for the accuracy of experimentally determined ZFS components, particularly for the systems characterized by odd spin quantum numbers.

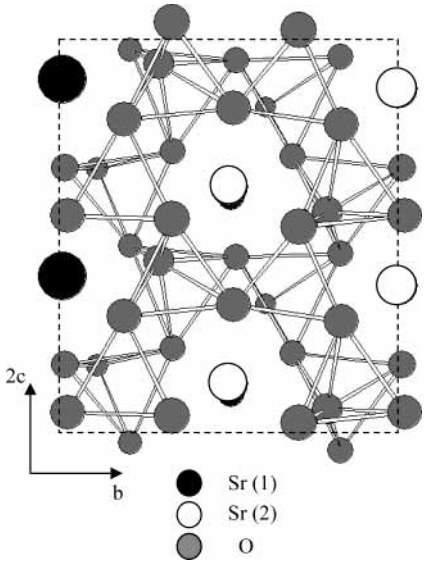

Figure 5. Projection of $SrAl_2O_4$ crystals in the bc plane.[26,27] The Sr ions lie in cavities composed of AlO_4 tetrahedra. For the simplicity, Al atoms are not shown here. The nearest neighbor distance between Sr ions is about 0.4 nm.

Determination of the Principal-Axis Orientation of the Second-Rank ZFS Tensor Based on the Superposition Model. In the previous section, the second-rank ZFS components were precisely determined in terms of the spectral analyses considering the fourth-order terms. Therefore, the empirical superposition model (SPM) is applicable to give the principal-axis orientation of the second-rank tensor. Also, the difference in signs of the *D* values for the Eu(1) and Eu(2) sites is discussed with the help of the SPM.

The essential assumption made in the SPM is that the ZFS is produced by sums of individual contributions from neighboring ligands.[18] In the context of the SPM, theoretical second-rank ZFS components are given as

$$b_k^q = \sum_i K_k^q(\theta_i,\phi_i)\bar{b}_k(R_i) \qquad (5)$$

where the summation is taken over all ligands *i*. And $K_k^q(\theta_i, \phi_i)$ stands for the so-called "coordination factor", which depends on the angular positions of ligands, and $\bar{b}_k(R_i)$ is the intrinsic parameter defined in the Appendix. Nakamura et al. also applied the SPM to an Eu(II)-doped strontium aluminate.[4b] Their analysis, however, did not succeed because they used the SPM parameters determined for other samples. As mentioned above, the Eu(1) and Eu(2) sites are substituted for two Sr sites in the $SrAl_2O_4$ host crystal. The projection of the crystal in the bc plane is shown in Figure 5.[26,27] The two Sr sites are denoted by closed and open circles, which are termed Sr(1) and Sr(2). The nearest neighbor distance between Sr ions is about 0.4 nm. Since Eu(II) ion has nearly the same ionic radius as Sr(II) ion, we can assume that there are no crystallographic distortions due to the substitution of the Eu(II) ions. The validity of this assumption is also supported by crystallographic data for $SrAl_2O_4$:Eu.[28] Therefore, we employed the X-ray powder diffraction (XRD) data of $SrAl_2O_4$ by Matsushima et al.[27] for the angular position. Theoretical ZFS parameters for the Eu(1) and Eu(2) sites were determined by eq 5 together with the crystallographic data, as described in the Appendix. Table 3 shows the theoretical *D* and *E* values. The result was in good agreement with the experimental values. Assuming the negative intrinsic parameter $\bar{b}_k(R_i)$ (see Appendix), we assigned the Eu(1) and Eu(2) sites to the Sr(1) and Sr(2) sites, respectively. This is the first assignment relating the ZFS parameters and the local structures for Eu(II)-doped strontium aluminates with the help of the SPM. Moreover, the principal-axis orientations of the second-rank ZFS tensors were for the first time determined in the frame of the SPM. Figure 6 shows the local structures around the Eu sites and the relative orientations anticipated from the SPM analysis. In Table 4, their direction cosines are shown. Since the intrinsic parameter $\bar{b}_k(R_i)$ is given to be negative for both sites, it is concluded that the signs of their *D* values depend on the structural factor $(3\cos^2\theta_i - 1)$ within the SPM. The different sign of *D* can be explained by the geometrical picture as shown in Figure 6: (a) the negative *D* value of the Eu(1) site corresponds to the prolate

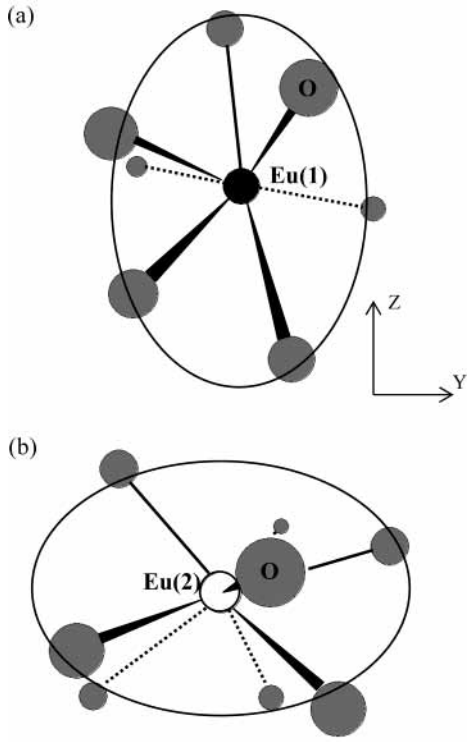

Figure 6. Spatial distribution of ligands around Eu(II) ions: (a) Eu-(1) site (prolate distribution); (b) Eu(2) site (oblate distribution). Only oxygen atoms nearer than 0.31 nm from the metal ion are considered here. The local site structures (a) and (b) correspond to those at the Sr(1) and Sr(2) sites in Figure 5, respectively. The principal axis orientations of the second-rank ZFS tensors determined by the SPM are illustrated on the right-hand side of the structures.

TABLE 3: Theoretical Second-Rank ZFS Components Based on the SPM

	Eu (1)		Eu (2)
b_2^0/cm^{-1}	−0.1422		0.1192
b_2^2/cm^{-1}	0.1227		0.0999
$\bar{b}_2(R_0)/\text{cm}^{-1}$	−0.1443		−0.1387
m		5.5	
n		8.4	
R_0/nm	0.2684		0.2746

TABLE 4: Direction Cosines of the Second-Rank ZFS Tensors Determined for the Eu(1) and Eu(2) Sites Based on the SPM

		a	b	c
Eu (1)	*X*	0.2132	−0.4593	−0.8623
	Y	0.7523	−0.4860	0.4449
	Z	−0.6243	−0.7435	0.2149
Eu (2)	*X*	−0.3433	−0.5535	0.7588
	Y	−0.8160	−0.2243	−0.5328
	Z	−0.4651	0.8021	0.3746

($3\cos^2\theta_i - 1 > 0$) spatial distribution of ligands and (b) the positive D value of Eu(2) site corresponds to the oblate distribution ($3\cos^2\theta_i - 1 < 0$).

Conclusions

In this work, the necessity of considering the fourth-order terms was discussed with the help of multifrequency EPR spectroscopy. The ZFS parameters were determined by the combined use of the perturbation treatment of the spin Hamiltonian and a spectral simulation based on the hybrid-eigenfield approach. A spectral analysis neglecting the fourth-order terms does not reproduce the whole experimental spectra including the extra lines arising from the $M_S = 1/2 \leftrightarrow -1/2$ transition. Moreover, the omission leads to the misevaluation of the E values. It is concluded that the fourth-order terms are crucial for the precise determination of the second-rank ZFS components. The empirical SPM was applied in order to determine the orientation of the principal-axes of the second-rank ZFS tensors with the respect to the crystallographic axes. For the first time, the relative orientations were determined for the Eu(II) ions doped in strontium aluminates. Also, the ZFS parameters were related to the local structures around the Eu(II) ions with the help of the crystallographic data of the host crystal.

Acknowledgment. We thank Prof. S. Matsushima of Kitakyushu National College of Technology, Japan, for supplying the crystallographic data for $SrAl_2O_4$. We are also very grateful to Professor T. Nakamura of Shizuoka University, Japan, for providing valuable discussion. This work has been partly supported by Grants-in-Aid for JSPS Fellows from the Ministry of Education, Culture, Sports, Science and Technology, Japan. One of the authors (H.M.) acknowledges Research Fellowships of the Japan Society for the Promotion of Science for Young Scientists.

Supporting Information Available: EPR spectra of the sample calculated at 180 GHz, where the importance of the fourth-order terms and the occurrence of the extra line are demonstrated. This material is available free of charge via the Internet at http://pubs.acs.org.

Appendix

Stevens Operators. There are some inconsistencies of notation for the Stevens operators in the literature as is comprehensively described by Rudowicz.[29,30] In this work, Newman's notation[18b] is utilized:

$$O_2^0 = 3S_z^2 - S(S+1) \tag{A1}$$

$$O_2^2 = \frac{1}{2}(S_+^2 + S_-^2) \tag{A2}$$

$$O_4^0 = 35S_z^4 - (30S(S+1) - 25)S_z^2 - 6S(S+1) + 3S^2(S+1)^2 \tag{A3}$$

$$O_4^2 = \frac{1}{4}\{7S_z^2 - S(S+1) - 5\}(S_+^2 + S_-^2) + \frac{1}{4}(S_+^2 + S_-^2)\{7S_z^2 - S(S+1) - 5\} \tag{A4}$$

$$O_4^4 = \frac{1}{2}(S_+^4 + S_-^4) \tag{A5}$$

The remaining operators are given in the literature.[18b] Also, the conventional **D** tensor can be expressed by the Stevens parameters b_k^q as follows:

$$\mathbf{D} = \begin{pmatrix} D_{XX} & D_{XY} & D_{XZ} \\ D_{XY} & D_{YY} & D_{YZ} \\ D_{XZ} & D_{YZ} & D_{ZZ} \end{pmatrix} = \frac{1}{6} \times \begin{pmatrix} -2(b_2^0 - b_2^2) & 2b_2^{-2} & b_2^1 \\ 2b_2^{-2} & -2(b_2^0 + b_2^2) & b_2^{-1} \\ b_2^1 & b_2^{-1} & 4b_2^0 \end{pmatrix} \tag{A6}$$

where $D_{XX} = -(D/3) + E$, $D_{YY} = -(D/3) - E$, $D_{ZZ} = 2D/3$, and $D_{XX} + D_{YY} + D_{ZZ} = 0$.

General Expression for Resonance Fields of Canonical Peaks Arising from $S = 7/2$ Spin System under First-Order Approximation. Because tensorial entities greater than rank two are not expressible as matrices, their angular variation cannot be calculated as simply as the conventional **D** tensor. Therefore, the following derivation was carried out with the help of the transformation property of the Stevens operators.[30] Also, for simplicity, we assumed an isotropic g value below. The shifts of the resonance field for the $M_S \leftrightarrow M_S - 1$ and $-M_S \leftrightarrow -M_S + 1$ transitions are given within a first-order approximation, in the case of $\mathbf{B} \parallel Z$ as

$$\begin{aligned} Del_1 &= B(+7/2 \leftrightarrow +5/2) - B(-5/2 \leftrightarrow -7/2) \\ &= -(12b_2^0 + 40b_4^0)/g\beta_e \\ Del_2 &= B(+5/2 \leftrightarrow +3/2) - B(-3/2 \leftrightarrow -5/2) \\ &= -(8b_2^0 - 20b_4^0)/g\beta_e \\ Del_3 &= B(+3/2 \leftrightarrow +1/2) - B(-1/2 \leftrightarrow -3/2) \\ &= -(4b_2^0 - 24b_4^0)/g\beta_e \end{aligned} \tag{A7}$$

where $B(M_S \leftrightarrow M_S - 1)$ stands for the resonance fields of the $M_S \leftrightarrow M_S - 1$ transition. In the case of $\mathbf{B} \perp Z$, the shifts are given as

$$\begin{aligned} Del_4 &= B(+7/2 \leftrightarrow +5/2) - B(-5/2 \leftrightarrow -7/2) \\ &= [6b_2^0 - 15b_4^0 - (6b_2^2 - 5b_4^2)\cos 2\phi - 5b_4^4\cos 4\phi + 5b_4^{-2}\sin 2\phi - 5b_4^{-4}\sin 4\phi]/g\beta_e \\ Del_5 &= B(+5/2 \leftrightarrow +3/2) - B(-3/2 \leftrightarrow -5/2) \\ &= \left[4b_2^0 - \frac{15}{2}b_4^0 - \left(4b_2^2 + \frac{5}{2}b_4^2\right)\cos 2\phi + \frac{5}{2}b_4^4\cos 4\phi - \frac{5}{2}b_4^{-2}\sin 2\phi + \frac{5}{2}b_4^{-4}\sin 4\phi\right]/g\beta_e \\ Del_6 &= B(+3/2 \leftrightarrow +1/2) - B(-1/2 \leftrightarrow -3/2) \\ &= [2b_2^0 - 9b_4^0 - (2b_2^2 + 3b_4^2)\cos 2\phi + 3b_4^4\cos 4\phi - 3b_4^{-2}\sin 2\phi + 3b_4^{-4}\sin 4\phi]/g\beta_e \end{aligned} \tag{A8}$$

where ϕ is the polar angle between the static magnetic field **B** and the X principal axis of the second rank ZFS tensor. Equations A7 and A8 are applicable to $S = 7/2$ spin systems in any symmetry fields. As is obvious from eq A8, the parameters b_4^{-2} and b_4^{-4} hardly influence the resonance fields of the canonical peaks because of their sine coefficients. Also, the remaining fourth-rank ZFS components such as $b_4^{\pm 1}$, which we must consider in the case of symmetry fields lower than

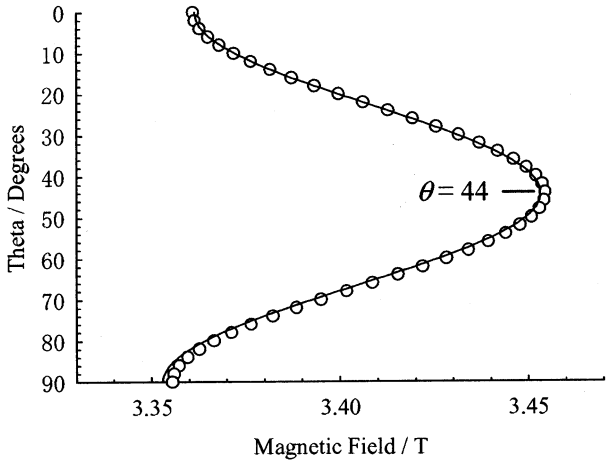

Figure 7. Angular variation of resonance fields calculated for the Eu-(1) site; $0 \le \theta \le \pi/2$, $\phi = \pi/2$. The calculation with the complete set of the parameters in Table 1 is illustrated by solid lines, which correspond to those in Figure 4b. A calculation with an incomplete set, neglecting the fourth-rank ZFS components in Table 1, is illustrated by open circles.

monoclinic, do not influence of the resonance fields. These parameters may be determined by careful analysis of extra lines observed in the X-band spectrum. Recently, estimation of the b_4^3 value from extra lines was discussed for *S*-state ions in trigonal symmetry by Priem et al.[31] In this work, however, significant shift caused by the odd terms was not seen in the observed X-band spectrum.

General Expression for Resonance Field of $M_S = 1/2 \leftrightarrow -1/2$ Transition Arising from $S = 7/2$ Spin System under Second-Order Approximation. To derive the general expression for the resonance field of $M_S = 1/2 \leftrightarrow -1/2$ transition, the spin Hamiltonian eq 3 is rewritten as

$$\hat{H} = g\beta_e M_S B + \sum_{k,q} f_k b_k^q(\theta,\phi) O_k^q (k = 2,4; |q| \le k) \quad \text{(A9)}$$

Here, $b_k^q(\theta,\phi)$ stands for angular-dependent ZFS parameters, which can be calculated by using the transformation property of the Stevens operators.[30] From the second-order perturbation treatment of the spin Hamiltonian, the general expression was derived for the first time in this work:

$$B = \frac{h\nu}{g\beta_e} + \sum_{q=-1,1} [25\{b_2^q(\theta,\phi)^2 - 4b_2^{2q}(\theta,\phi)^2\} - 30\{3b_2^q(\theta,\phi) \times b_4^q(\theta,\phi) + 14b_2^{2q}(\theta,\phi) \times b_4^{2q}(\theta,\phi)\} + 3\{27b_4^q(\theta,\phi)^2 - 47b_4^{2q}(\theta,\phi)^2 + 2b_4^{3q}(\theta,\phi)^2 - 14b_4^{4q}(\theta,\phi)^2\}] \times \frac{1}{60(g\beta_e)^2 B} \quad \text{(A10)}$$

The resonance field depends mainly on the square of each ZFS parameter differently from the positions of the other transitions. Therefore, as predicted in the previous work,[25] it is obvious that the field position of the $M_S = 1/2 \leftrightarrow -1/2$ transition is hardly influenced by the fourth-order terms. This is also supported by exact numerical calculation. Figure 7 shows the angular variation of resonance fields calculated for the $M_S = 1/2 \leftrightarrow -1/2$ transition arising from the Eu(1) site. Solid lines in Figure 7 correspond to those in Figure 4b. Also, open circles stand for the angular variation calculated for the Eu(1) site by using only *g* and second-order ZFS terms in Table 1. In addition to the prediction based on eq A10, the figure demonstrates that the field position is almost independent of the fourth-order terms.

Superposition Model (SPM). In the frame of the SPM, the second-rank ZFS components is given by

$$b_2^0 = \frac{1}{2}\sum_i (3\cos^2\theta_i - 1)\bar{b}_2(R_i) = D \quad \text{(A11)}$$

$$b_2^2 = \frac{3}{2}\sum_i \sin^2\theta_i \cos 2\phi_i \bar{b}_2(R_i) = 3E \quad \text{(A12)}$$

$$b_2^1 = 3\sum_i \sin 2\theta_i \cos\phi_i \bar{b}_2(R_i) = 6D_{xz} \quad \text{(A13)}$$

$$b_2^{-1} = 3\sum_i \sin 2\theta_i \sin\phi_i \bar{b}_2(R_i) = 6D_{yz} \quad \text{(A14)}$$

$$b_2^{-2} = \frac{3}{2}\sum_i \sin^2\theta_i \sin 2\phi_i \bar{b}_2(R_i) = 3D_{xy} \quad \text{(A15)}$$

where $D_{xx} = -D/3 + E$, $D_{yy} = -D/3 - E$, $D_{zz} = 2D/3$, and the structural factor is the function of the real spherical harmonics $Y_k^q(\theta_i, \phi_i)$. Here, the intrinsic parameter depends on the bond length R_i between the ligands and the metal ion. According to Newman et al.,[18] the distance dependence is described as

$$\bar{b}_k(R_i) = -A\left(\frac{R_0}{R_i}\right)^m + B\left(\frac{R_0}{R_i}\right)^n \quad \text{(A16)}$$

where the exponents, *m* and *n*, are empirical parameters. Also, the average distance between the ligands and metal ion in each site was used as the reference distance R_0. The parameter $\bar{b}_k(R_0)$ commonly used in the literature is equal to $(-A + B)$.[32] It is empirically known that the parameter $\bar{b}_k(R_0)$ produces nearly the same value among systems with the same combination of the metal and ligands.[18] Therefore, we assumed $-0.17 < \bar{b}_2(R_0)/\mathrm{cm}^{-1} < -0.07$, according to the Newman's result.[32] Moreover, we assumed that $\bar{b}_k(R_i)$ exhibits the identical distance dependence between the two Eu sites because they exist in the same host crystal.

References and Notes

(1) (a) Takui, T.; Sato, K.; Shiomi, D.; Itoh, K. In *Magnetic Properties of Organic Materials*; Lahti, P. M., Ed.; Marcel Dekker: New York, 1999; Chapter 11. (b) Takui, T.; Itoh, K. In *Molecular Magnetism; New Magnetic Materials*; Itoh, K., Kinoshita, M., Eds.; Kodansha and Gordon & Breach: Tokyo and Amsterdam, 2000; Chapter 3. (c) Takui, T.; Matsuoka, H.; Furukawa, K.; Nakazawa, S.; Sato, K.; Shiomi, D. In *EPR of Free Radicals in Solids: Trends in Methods and Applications*; Lund, A., Shiotani, M., Eds.; Kluwer Academic Publishers: Boston, 2003; Chapter11.

(2) Abragam A.; Bleaney, B. *Electron paramagnetic resonance of transition ions;* Dover Publications: New York, 1986.

(3) Pilbrow, J. R. *Transition Ion Electron Paramagnetic Resonance;* Clarendon Press: Oxford, 1990.

(4) (a) Nakamura, T.; Matsuzawa, T.; Rowlands, C. C.; Beltrán-López, V.; Smith, G. M.; Riedi, P. C. *J. Chem. Soc., Faraday Trans.* **1998**, *94*, 3009−3012. (b) Nakamura, T.; Kaiya, K.; Takahashi, N.; Matsuzawa, T.; Rowlands, C. C.; Beltrán-López, V.; Smith, G. M.; Riedi, P. C. *Phys. Chem. Chem. Phys.* **1999**, *1*, 4011−4014. (c) Kaiya, K.; Takahashi, N.; Nakamura, T.; Matsuzawa, T.; Smith, G. M.; Riedi, P. C. *J. Lumin.* **2000**, *87*−*89*, 1073−1075. (d) Nakamura, T.; Kaiya, K.; Takahashi, N.; Matsuzawa, T.; Rowlands, C. C.; Beltrán-López, V.; Smith, G. M.; Riedi, P. C. *J. Mater. Chem.* **2000**, *10*, 2566−2569. (e) Nakamura, T.; Takeyama, T.; Takahashi, N.; Jagannathan, R.; Karthikeyani, A.; Smith, G. M.; Riedi, P. C. *J. Lumin.* **2003**, *102*−*103*, 369−372.

(5) Miyamoto, R.; Sudoh, S. *Bull. Chem. Soc. Jpn.* **1995**, *68*, 3439−3443.

(6) Cugunov, L.; Mednis, A.; Kliava, J. *J. Phys. Condens. Matter* **1991**, *3*, 8017−8025.

(7) Nicklin, R. C.; Johnstone, J. K.; Barnes, R. G.; Wilder, D. R. *J. Chem. Phys.* **1973**, *59*, 1652−1668.

(8) Szyczewski, A.; Lis, S.; Kruczynski, Z.; But, S. *J. Alloys Compound* **2002**, *341*, 307−311.

(9) (a) Sato, K.; Matsuoka, H.; Shiomi, D.; Takui, T.; Itoh, K. *Mol. Cryst. Liq. Cryst.* **1999**, *334*, 1045−1054. (b) Matsuoka, H.; Sato, K.; Shiomi, D.; Takui, T. *Synth. Met.* **2001**, *121*, 1822−1833. (c) Matsuoka, H.; Sato, K.; Shiomi, D.; Takui, T. *Appl. Magn. Reson.* **2003**, *23*, 517−538.

(10) Matsuoka, H.; Furukawa, K.; Sato, K.; Shiomi, D.; Kojima, Y.; Hirotsu, K.; Furuno, N.; Kato, T.; Takui, T. *J. Mater. Res.*, submitted.

(11) Sato, K. Doctoral Thesis, Osaka City University, Osaka, 1994.

(12) Teki, Y.; Fujita, I.; Takui, T.; Kinoshita, T.; Itoh, K. *J. Am. Chem. Soc.* **1994**, *116*, 11499−11505.

(13) Eremin, M. V.; Antonova, I. I. *J. Phys. Condens. Matter* **1998**, *10*, 5567−5575 and references therein.

(14) Pryce, M. H. L. *Phys. Rev.* **1950**, *80*, 1107−1108.

(15) (a) Kondo, J. *Progr. Theor. Phys.* **1960**, *23*, 106−114. (b) Novak, P.; Veltrusky, I. *Phys. Status Solidi B* **1976**, *73*, 575−856. (c) Emery, J.; Leble, A.; Fayey, J. C. *J. Phys. Chem. Solids* **1981**, *42*, 789−798.

(16) (a) Heuvelen, A. V. *J. Chem. Phys.* **1967**, *46*, 4903−4905. (b) Dreybrodt, W.; Silber, D.; *Phys. Status Solidi* **1969**, *34*, 559−568.

(17) (a) Sharma, R. R.; *Phys. Rev. A* **1968**, *176*, 467−478. (b) Yu, W. L.; Zhao, M. G.; Lin, Z. Q. *J. Phys. C: Solid State Phys.* **1985**, *18*, 1857−1863. (c) Yu, W. L.; Zhao, M. G. *Phys. Rev. B* **1988**, *37*, 9254−9267.

(18) (a) Bradbury, M. I.; Newman, D. J. *Chem. Phys. Lett.* **1967**, *1*, 44−45. (b) Newman, D. J.; Urban, W. *Adv. Phys.* **1975**, *24*, 793−843. (c) *Rep. Prog. Phys.* **1989**, *52*, 699−763. (d) *Crystal Field Handbook;* Newman, D. J., Ng, B., Eds.; Cambridge University Press: Cambridge, 2000.

(19) (a) Reynolds, R. W.; Boatner, L. A.; Finch, C. B.; Chatelain, A.; Abraham, M. M. *J. Chem. Phys.* **1972**, *56*, 5607−5625. (b) Rappaz, M.; Boatner, L. A.; Abraham, M. M. *J. Chem. Phys.* **1980**, *73*, 1095−1103. (c) Rappaz, M.; Abraham, M. M.; Ramey, J. O.; Boatner, L. A. *Phys. Rev. B* **1981**, *23*, 1012−1030. (d) The parameter b_4^2 was not considered in (a)−(c). Also, computer simulation of experimental powder-pattern EPR spectra was not carried out there.

(20) Koopmans, H. J. A.; Perik, M. M. A.; Nieuwenhuljse, B. *Phys. Status Solidi B* **1984**, *122*, 317−330.

(21) Matsuoka, H.; Sato, K.; Shiomi, D.; Kojima, Y.; Hirotsu, K.; Furuno, N.; Takui, T. In *EPR in the 21st Century: Basics and Applications to Materials, Life and Earth Sciences;* Kawamori, A., Yamauchi, J., Ohta, H., Eds.; Elsevier: Amsterdam, 2002; p 264.

(22) Belford, G. G.; Belford R. L.; Bukhalter, J. F. *J. Magn. Reson.* **1973**, *11*, 251−265.

(23) Cugunov, L.; Mednis, A.; Kliava, J. *J. Magn. Reson. A* **1994**, *106*, 153−158.

(24) Belford R. L.; Nilges, M. J. Presented at EPR Symposium 21st Rocky Mountain Conference, Denver, Colorado, 1979.

(25) Teki, Y.; Takui, T.; Itoh, K. *J. Chem. Phys.* **1988**, *88*, 6134−6145.

(26) (a) Schulze, V. A.-R.; Müller-Buschbaum, Hk. *Z. Anorg. Allg. Chem.* **1981**, *475*, 205−210. (b) The crystallographic data reproted in (a) included a relatively large R-factor.

(27) (a) Matsushima, S.; Nakamura, H.; Arai, M.; Xu, C.-N. *Chem. Lett.* **2002**, 700−701. (b) Fractional coordinates for $SrAl_2O_4$ are not given in (a). (c) An R-factor less than 0.05 was obtained in (a).

(28) Wang, D.; Yin, Q.; Li, Y.; Wang, M. *J. Lumin.* **2002**, *97*, 1−6.

(29) Rudowicz, C. *Magn. Reson. Rev.* **1987**, *13*, 1−89.

(30) Rudowicz, C. *J. Phys. C: Solid State Phys.* **1985**, *18*, 1415−1430.

(31) Priem, A.; van Bentum, P. J. M.; Hagen, W. R.; Reijerse, E. J. *Appl. Magn. Reson.* **2001**, *21*, 535−548.

(32) Newman, D. J.; Urban, W. *J. Phys. C: Solid State Phys.* **1972**, 5, 3101−3109.

(33) (a) Nadzhina, T. N.; Pobedimskaya, E. A.; Belov, N. V. *Kristallogr.* **1976**, 21, 826−828. (b) Nadzhina, T. N.; Pobedimskaya, E. A.; Belov, N. V. *Kristallogr.* **1980**, 25, 938−943.